# Enhancement of excitonic and defect-related luminescence in neutron transmutation doped β-$Ga_2O_3$

Curtis P. Irvine,[1] Attila Stopic,[2] Mika T. Westerhausen,[1] Matthew R. Phillips,[1] and Cuong Ton-That[1,*]

[1]*School of Mathematical and Physical Science, University of Technology Sydney, Ultimo, NSW 2007, Australia*

[2]*ANSTO, Lucas Heights, NSW 2234, Australia*

[*]Corresponding author: cuong.ton-that@uts.edu.au

## Abstract

Neutron irradiation analysis, inductively coupled plasma mass spectrometry (ICP-MS) and cathodoluminescence (CL) spectroscopy are used to investigate the influence of transmuted Ge incorporation on the luminescence properties of β-$Ga_2O_3$ single crystals. Calculations based on $Ga_2O_3$-neutron interaction reveal temporal variations of both Ge and Zn concentrations as a function of time during and after neutron irradiation. To produce a concentration of $5 \times 10^{18}$ Ge donors/cm$^3$ from the neutron transmutation of Ga, the β-$Ga_2O_3$ crystal was irradiated for 27 hours, which was accompanied by the incorporation of $10^{16}$ Zn acceptors/cm$^3$. These calculated dopant concentrations are confirmed by ICP-MS chemical analysis. The β-$Ga_2O_3$ crystals exhibit a UV at 3.40 eV due to self-trapped holes (STHs) and two blue donor – acceptor pair (DAP) peaks at 3.14 eV (BL1) and 2.92 eV (BL2). In addition to the neutron-induced incorporation of substitutional Ge donors and Zn acceptors on Ga sites, Ga vacancies ($V_{Ga}$) were created by high-energy neutrons in the flux, which strongly enhanced the BL1 peak causing a large red shift of ~120 meV in the overall CL emission at 80 K. The $V_{Ga}$ acceptors charge compensate the neutron-induced Ge donors, making the $Ga_2O_3$ crystal highly resistive. Concurrent temperature-resolved CL measurements of the β-$Ga_2O_3$ before and after neutron irradiation reveal a twofold increase in both the STH and BL1 peaks. This result suggests that STHs are preferentially localized at an O site adjacent to $V_{Ga}$, as theoretically

predicted by Kananen *et al.* [Appl. Phys. Lett. 110, 202104 (2017)]. Analysis of the $Ga_2O_3$ CL temperature dependence reveals that the UV and BL1 bands after the neutron irradiation exhibit an equivalent activation energy of 100 ± 10 meV due to the presence of a neutron-induced defect that acts as an efficient competitive non-radiative recombination channel. The results also provide evidence that the BL1 and BL2 bands arise from different DAP pairs.

Keywords: gallium oxide; neutron irradiation; self-trapped exciton; vacancy defects; cathodoluminescence

## I. INTRODUCTION

Due to its ultrawide bandgap (4.9 eV), large breakdown electric field and radiation hardness, β-$Ga_2O_3$ is currently attracting great interest for use in electrical components for high-voltage and high-temperature operation, UV opto-electronics, as well as electronics in harsh surroundings, such as devices for extra-terrestrial and nuclear reactor technologies.[1] However, only unipolar n-type $Ga_2O_3$ based devices have been fabricated so far because p-type doping at sufficiently high levels remains problematic. Conversely, controllable n-type doping of $Ga_2O_3$ has been achieved by the in-growth incorporation of Si, Sn, Ge or H donors with activation energies ($E_a$) in the range of 16 to 60 meV.[2-5] These donors, as impurities, are considered to be likely candidates for the cause of the observed characteristic n-type conductivity in undoped $Ga_2O_3$ and can contribute to the low p-type doping efficiencies as acceptor compensators. There are two non-equivalent Ga atomic sites in β-$Ga_2O_3$ that are available for substitutional cation doping, Ga(I) and Ga(II) with tetrahedral and octahedral coordination geometry, respectively. Density functional theory (DFT) calculations show that Si and Ge donors preferentially occupy the Ga(I) site and act as shallow donors.[6] However, both shallow ($E_a$ = 34.9 meV) and deep donor ($E_a$ = 120 meV) states were found in Si-doped (010) β-$Ga_2O_3$ films grown by metal organic chemical vapor deposition.[7] Neal *et al.* reported

deep donors with ionization energies of 110 and 131 meV in commercial undoped (-201) β-$Ga_2O_3$ crystals from temperature dependent Hall effect and capacitance spectroscopy measurements.[8,9] Both these donor ionization energies were both tentatively attributed to Si donors occupying the Ga(II) site, with the disparity in the donor energy being due to the use of different measurement techniques.[8,10].

Photoluminescence (PL) and cathodoluminescence (CL) spectroscopy measurements of high-quality β-$Ga_2O_3$ single crystals and epilayers show a broad emission band that contains a UV band at 3.3 eV and blue luminescence (BL) bands at ~ 3.1 and ~ 2.8 eV; these bands have been attributed to self-trapped holes (STHs) and donor-acceptor pair transitions, respectively.[11-14] Cation vacancies are typically compensating acceptor defects in oxide semiconductors. Accordingly, Ga vacancies ($V_{Ga}$) are predicted to act as acceptors in β-$Ga_2O_3$ and are expected to play a critical role in the effort to achieve stable p-type doping and facilitate the fabrication of bipolar β-$Ga_2O_3$ devices. To date, however, the optical and electrical properties of vacancy defects in β-$Ga_2O_3$ bulk crystals have been subject of much debate. Theoretical calculations by Ingebringsten *et al.* [15] reported that a $Ga_i$ - $V_{Ga}$ pair complex with three different structural configurations, labelled $V_{Ga}^{ia}$, $V_{Ga}^{ib}$ and $V_{Ga}^{ic}$, have low formation energies in n-type $Ga_2O_3$ and so are likely to be abundant deep acceptors. The split $V_{Ga}$ modelling results have been supported by recent experiments.[16,17] Conversely, $Ga_i$ shallow donors were found to have a high formation energy, forming split energy levels at least 0.6 eV below the conduction band due to local atomic distortions.[15]

Neutron transmutation doping is an established semiconductor doping technique that enables precise dopant concentrations with a highly uniform spatial distribution. For example, this technique has been used to homogenously incorporate Ge in bulk GaN by the conversion of Ga into Ge after the capture of thermal neutrons. However, these $Ge_{Ga}$ dopants in GaN could not be electrically activated even after annealing at 1000°C, which was attributed to a structural

displacement of $Ge_{Ga}$ sites caused by the emission of nuclear particles.[18,19] Son *et al.* observed no neutral donor state in Si-doped $Ga_2O_3$ using electron spin resonance (ESR) spectroscopy and proposed that Si behaves like a DX-like donor state,[20] which is a defect complex formed between the Si donor and an lattice defect labelled X. This DX-like complex was found to be highly stable and only be partially activated after annealing at 1100°C.[20] Studies of neutron and proton irradiation effects in $Ga_2O_3$ crystals and epilayers report the creation of several electrically active defect states across the entire bandgap, although considerable controversy remains regarding the nature of defects induced by the irradiation.[21-24] Significantly, neutron irradiation has recently been used to homogenously introduce $V_{Ga}$ in β-$Ga_2O_3$.[21,25,26] The photocurrent in $Ga_2O_3$-based Schottky diodes was found to be strongly enhanced after neutron irradiation, which was explained by the introduction of $V_{Ga}$-related defects acting as hole traps.[27] EPR investigations of neutron-irradiated β-$Ga_2O_3$ reveal a hyperfine interaction of a trapped hole with two Ga neighboring atoms where the hole was found to be localized at a threefold-coordinated O site adjacent to $V_{Ga}$.[26] Studies of edge-defined film-fed (EFG) $Ga_2O_3$ crystals by DLTS and deep level optical spectroscopy enabled the identification of a defect state associated with fast neutron irradiation at 1.29 eV below the conduction band edge.[23] Gao *et al.*[25,28] used CL to investigate $Ga_2O_3$ films grown by pulsed laser deposition (PLD) and low-pressure chemical vapor deposition (LPCVD). These studies reported broad emission bands centred at 3.0 and 2.5 eV, which increase in intensity after neutron irradiation, suggesting that $V_{Ga}$ is involved in their transitions. Notably, the peak positions of these bands are different from the UV and BL bands observed in EFG-grown crystals. In this paper, we report a strong luminescence enhancement in β-$Ga_2O_3$ crystals following neutron irradiation. It is shown that $Ga_2O_3$ can be homogeneously doped with a precise Ge dopant concentration by thermal neutrons; however, the incorporated Ge donors are found to be strongly compensated by $V_{Ga}$ acceptors produced

by the presence of fast neutrons in the thermal neutron flux. Our results provide evidence for the involvement of $V_{Ga}$ in the both STH-related UV and blue defect emission peaks in neutron irradiated β-$Ga_2O_3$.

## II. EXPERIMENTAL DETAILS

The samples used in this study are unintentionally doped (UID) $Ga_2O_3$ 10 × 15 × 0.68 $mm^3$ crystals grown by the EFG method (Tamura Corporation, Japan). The crystal possesses the (-201) surface plane orientation and have been found to contain impurities of Si, Ir and Al.[29] The crystal was placed inside an Al capsule and exposed to neutrons for 27 hours in the irradiation facility in the OPAL Research Reactor at Australia's Nuclear Science and Technology Organisation (ANSTO).[30] The fluences of fast (energy > 0.5 MeV) and thermal neutrons (energy ~ 25 meV) were ~ $1.03 \times 10^{18}$ $cm^{-2}$ and $1.25 \times 10^{19}$ $cm^{-2}$ respectively. Fast neutrons are used to induce vacancy formation, and thermal neutrons cause the transmutation of Ga into Ge. Notably, these neutron exposure conditions are similar to the irradiation conditions previously used to produce $V_{Ga}$.[26] The mean free path of fast neutrons in the energy range of 1 eV – 20 MeV in $Ga_2O_3$ is > 1 cm,[31] which is significantly greater than the EFG crystal thickness of 0.68 mm. Before characterization studies were carried out, the irradiated crystal was left to decay for 11 months due to remnant radioactivity of unstable $^{192}$Ir. Quantitative analysis of neutron-induced transmuted impurities was conducted using laser ablation inductively coupled plasma mass spectrometry (LA-ICP-MS) using a New Wave Research NWR-193 excimer laser (Kennelec Scientific) coupled to an Agilent Technologies 7900 series ICP-MS. Laser ablation was conducted by ablating 20 1-mm lines using a 193 nm laser with a 150 μm spot scanning at 150 $\mu m.s^{-1}$ and pulsed at 40 Hz. Prior to data acquisition, the lines were pre-ablated to remove any surface contamination. Standard reference materials NIST 610 and NIST 612 were used for the calibration of ICP-MS. A NanoMagnetics Instruments *ezHEMS* system with a measurement limit of $10^9$ Ω.cm was used for electrical

characterization. CL spectroscopy was performed using an FEI Quanta 200 scanning electron microscope (SEM) equipped with a custom CL spectroscopy setup, consisting of a parabolic mirror light collector and an Ocean Optics QE65000 spectrometer. Temperature dependent measurements were performed by mounting the $Ga_2O_3$ samples on an Oxford Instruments liquid nitrogen cold stage allowing low temperature measurements from 80 to 300 K. All spectra were corrected for the total response of the CL measurement system. The electron beam current was measured using a Faraday cup in the sample stage.

## III. RESULTS AND DISCUSSION

### A. Neutron transmutation doping of $Ga_2O_3$

Neutron transmutation doping is a well-known method that produces homogenous doping in bulk semiconductors with high precision.[32] $Ga_2O_3$ contains natural isotopes $^{69}$Ga and $^{71}$Ga with natural abundances of 60.2% and 39.8%, respectively. Unstable isotopes are formed from these Ga isotopes following exposure to neutron irradiation through the capture of thermal neutrons ($n$) and their subsequent decay to stable isotopes as follows:[33]

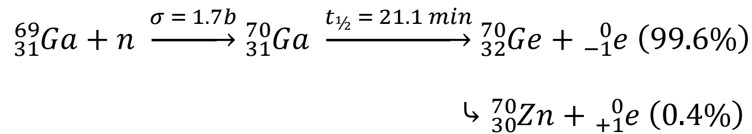

$$^{69}_{31}Ga + n \xrightarrow{\sigma = 1.7b} {}^{70}_{31}Ga \xrightarrow{t_{½} = 21.1\,min} {}^{70}_{32}Ge + {}^{0}_{-1}e \ (99.6\%)$$

$$\hookrightarrow {}^{70}_{30}Zn + {}^{0}_{+1}e \ (0.4\%)$$

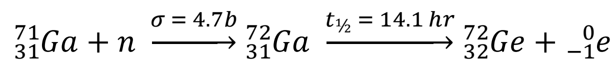

$$^{71}_{31}Ga + n \xrightarrow{\sigma = 4.7b} {}^{72}_{31}Ga \xrightarrow{t_{½} = 14.1\,hr} {}^{72}_{32}Ge + {}^{0}_{-1}e$$

where σ is the neutron capture cross section at 25.3 meV and $t_{½}$ is the lifetime calculated using Evaluated Nuclear Data Format (ENDF) and NUDAT data libraries.[34] Unstable isotope $^{70}$Ga can either beta decay to $^{70}$Ge (99.6% probability) or electron capture to $^{70}$Zn (0.4% probability) with $t_{½}$ = 21.1 mins. $^{72}$Ga beta decays with $t_{½}$ = 14.1 hours. The above parameters and an applied thermal neutron flux of $1.1 \times 10^{14}$ cm$^{-2}$s$^{-1}$ were used to calculate the concentration of transmutation Ge impurities according standard equations.[33] The computed Ge concentration (the sum of $^{70}$Ge and $^{72}$Ge isotopes) produced as a function of time during and after neutron

irradiation are shown in Fig. 1(a, b). The Ge concentration shows significant temporal dependence on the time scale of days, which should be taken into consideration for experimental study of neutron irradiated $Ga_2O_3$ systems. The Ge concentration grows significantly within the first 5 days post irradiation due to the decay of the unstable $^{70}$Ga and $^{72}$Ga, which remains constant at $1.7 \times 10^{18}$ atoms/cm$^3$ afterward. The primary acceptor dopant formed in neutron irradiated $Ga_2O_3$ is Zn, its concentration is found to increase substantially as unstable Ga and Cu isotopes decay and Zn is produced. The calculated Zn concentrations as a function of irradiation and post-irradiation time are presented in Supplemental Material Fig. S1.[35] The total Zn concentration post irradiation is $7.3 \times 10^{15}$ atoms/cm$^3$ for 27 hours irradiation as depicted in Fig. S1(b).

Chemical analysis was conducted using ICP-MS to experimentally validate the transmutation calculation results. Raw ICP-MS signal traces in counts per second (cps) for the isotopes $^{70}$Ge and $^{72}$Ge in the crystal before and after neutron irradiation are shown in Fig. 1(c, d). Each of the traces contains a stable plateau phase where the ablated material is constantly carried to the ICP-MS; the signal from this plateau is used for quantitative analysis. Isotopes $^{70}$Ge and $^{70}$Zn cannot be distinguished due to spectral overlaps; however, the intensity increase in Fig. 1(c) following neutron irradiation arises mostly (99.6%) from the formation of $^{70}$Ge as shown in the above decay equations. The $^{72}$Ge signal in the pristine $Ga_2O_3$ during laser ablation is only slightly higher than the laser-off background and its corresponding Ge concentration is about 0.13 ppm ($7.0 \times 10^{15}$ atoms/cm$^3$). After the neutron irradiation, the $^{72}$Ge intensity increases by three orders of magnitude and the measured Ge concentration in the irradiated crystal, averaged over 19 scans, is $97.5 \pm 1.9$ ppm ($5.2 \pm 0.1 \times 10^{18}$ atoms/cm$^3$). Notably, this measured Ge concentration in the neutron irradiated $Ga_2O_3$ is significantly higher than the calculated value, likely due to the matrix mismatch between the ICP-MS standards and $Ga_2O_3$ crystal; however, the exact source of discrepancy is beyond the scope of this work. The flat

plateau shape of the ICP-MS profiles confirms that Ge is uniformly incorporated in the crystal. The crystal was also found to contain the expected Sn and Si impurities in a few parts per million (~$10^{17}$ atoms/$cm^3$) range,[29] and the concentrations of these donors were unchanged following the neutron irradiation. From the Hall measurements, the carrier concentration of the pristine crystal was determined to be $2 \times 10^{17}$ $cm^{-3}$. Zn impurities were detectable by ICP-MS in both the pristine and irradiated crystals. The Zn isotope traces, shown in Fig. S1(c, d), all have signal intensities less than $5 \times 10^2$ cps. The $^{66}$Zn and $^{68}$Zn traces are considered to be equivalent for the pristine and irradiated crystals within the measurement uncertainty. The total measured Zn concentration is estimated to be ~ $10^{16}$ $cm^{-3}$ for both the crystals, consistent with the calculated transmuted Zn concentration. It is noted that the EFG $Ga_2O_3$ crystals used in this study contain a number of different metal impurities with concentrations up to 1 ppm, including Fe, Al, Cr and Ir.[29] The amount of Zn measured by ICP-MS in this work is about 0.3 ppm, which is not dissimilar to the concentrations of the reported metal impurities. The neutron-irradiated crystal is highly resistive, and its conductivity at room temperature could not be measured reliably due to the lower measurement limit of the electrometer, suggesting that Ge donors are strongly compensated by neutron-induced defects and Zn acceptors.

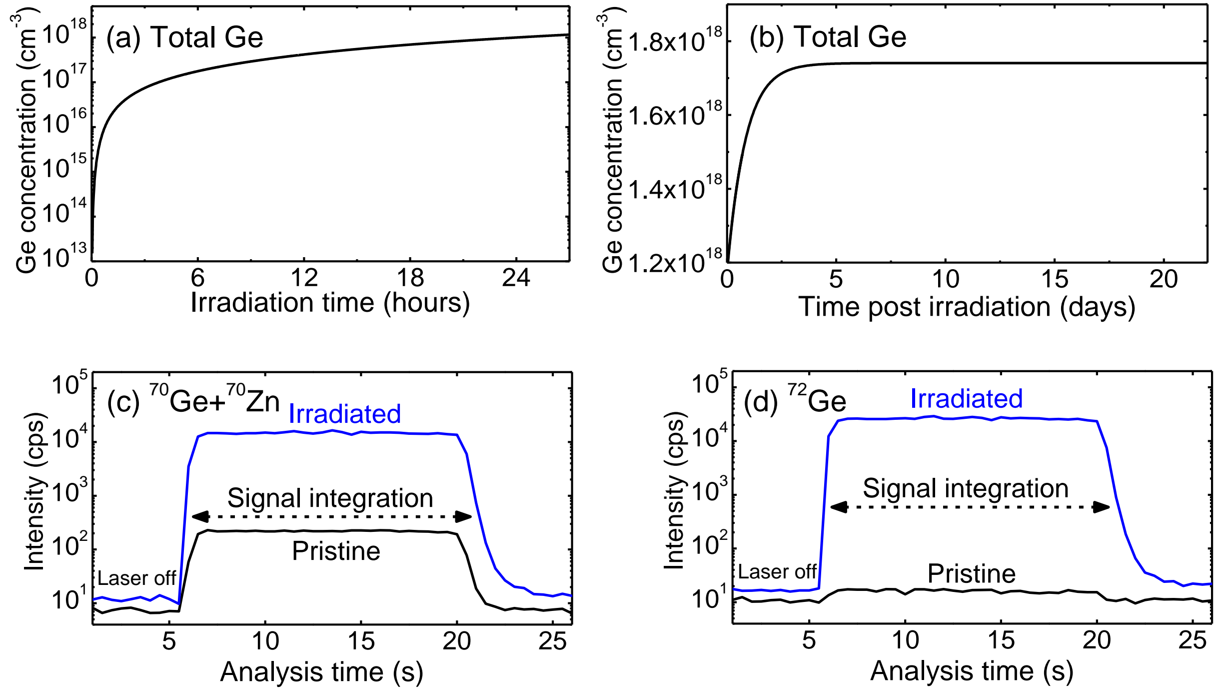


**Figure 1.** (a) Calculated temporal transmuted Ge concentration in β-$Ga_2O_3$ with irradiation time. After 27 hours irradiation the crystal is doped with $1.2 \times 10^{18}$ $cm^{-3}$ Ge atoms/$cm^3$. (b) Calculated temporal transmuted Ge concentration as a function of time following the neutron irradiation. The Ge concentration increases within the first 5 days post irradiation and remains constant at $1.7 \times 10^{18}$ atoms/$cm^3$ afterward. (c, d) ICP-MS signal traces for isotopes $^{70}$Ge, $^{70}$Zn and $^{72}$Ge from the laser ablation of the pristine and 27-hours irradiated $Ga_2O_3$ crystals. Isotopes $^{70}$Ge and $^{70}$Zn cannot be distinguished due to spectral overlaps; however, the intensity increase following neutron irradiation is mostly (99.6%) due to the creation of $^{70}$Ge isotope. The $^{72}$Ge signal intensity increase by three orders of magnitude upon the neutron irradiation.

### B. Neutron irradiation effects on luminescence properties

Normalized temperature-resolved CL spectra acquired from the β-$Ga_2O_3$ crystal under identical excitation conditions (15 kV, 3.8 nA) before and after neutron irradiation at 80 and 280 K are shown in Fig. 2(a) and (b), respectively. As discussed below, the β-$Ga_2O_3$ CL spectra contains an intrinisic UV emission as well two defect-related peaks in the blue spectral region. At 80 K, the CL emission peak of the entire CL spectrum located at 3.27 eV in the irradiated sample is redshifted by 120 meV compared with emission maximum observed in the pristine crystal. This irradiation-induced redshift and associated CL emission broadening are caused by

an increase in the blue emission, compared with the intrinsic UV band, which is attributed to the creation of additional $V_{Ga}$ defects. Conversely, Fig 2(b) shows that the CL emission peak positions and shapes of the pristine and irradiated crystals at 280 K are identical due to complete thermal quenching of the STH UV emission. Previous studies of Zn-doped β-$Ga_2O_3$ show that a CL emission band at 2.7 eV is strongly influenced by the Zn incorporation.[36] However, no additional CL emission peaks appear over the entire temperature range up to 300 K after neutron irradiation due to incorporated Zn acceptors most likely due to its low $10^{16}$ $cm^{-3}$ concentration. The insets of Figs 2(a, b) also show the as-measured CL spectra at 80 and 280 K, revealing a luminescence enhancement at 80 K with the emission intensity increasing by a factor of more than two, which is ascribed to additional $V_{Ga}$ defects produced by the irradiation. This luminescence enhancement is remarkable as radiation-induced defect formation in semiconductors normally quenches the pre-existing luminescence. As temperature increases, the CL emission of the irradiated crystal is quenched more rapidly than the pristine counterpart due to the thermal activation of non-radiative defects created by the neutron irradiation. Eventually at 280 K, the irradiated to pristine emission intensity ratio has decreased to 0.3 [see the inset in Fig. 2(b)] from its value of 2 at 80 K. Notably, previous investigations of neutron irradiated β-$Ga_2O_3$ by other workers have confirmed the formation of deep-level defects after fast neutron irradiation.[23] Fig. S2(a, b) present plots of the CL peak position and overall full width at half maximum (FWHM) respectively collected from the pristine and irradiated β-$Ga_2O_3$ over the temperature range of 80 – 300 K, showing that the spectra are red shifted and broadened post irradiation across the entire temperature range. The FWHM of the emission from both the pristine and irradiated crystals steadily increases with rising temperature. The CL emission peak from the pristine crystal shifts rapidly towards lower energy with increasing temperature due to the thermal quenching of the STH UV emission. In

contrast, the CL red shift in the irradiated crystal with temperature is minimal due to enhanced thermal stability of STH UV peak caused by additional $V_{Ga}$ defects.

In β-$Ga_2O_3$, holes can be trapped into strongly lattice coupled polaron states that can relax radiatively producing a broad Gaussian-like emission band.[11,12] Compared with the PL emission profile of the STH in β-$Ga_2O_3$ single crystals (peak energy E = 3.37 eV, FWHM = 0.62 eV),[37] the measured CL spectra are significantly broader [see Fig. S2(b)], indicating that additional defect-related emission is present in these spectra. In order to extract physically meaningful results from the CL spectra with highly overlapped peaks, spectral deconvolution was performed using conventional peak fitting techniques using the following procedure. First, the STH peak was fitted to the high energy side of the spectrum using the peak position and FWHM reported for an isolated STH emission peak [37] (as shown in Fig. 2(c)) before deconvoluting the complete spectrum. Using this approach, the low energy side of the emission spectrum was fitted with two broad defect-related Gaussian peaks labelled BL1 and BL2 using seed values from the literature (BL1: E = 3.14 eV, FWHM = 0.60 eV; BL2: 2.92 eV, 0.65 eV).[11,38] The BL1 peak energy matches closely with the peak position found in the difference spectrum (Fig. S3), which is achieved by the subtraction of the pristine spectrum from the irradiated spectra after the pristine spectrum is scaled by 1.7 to account for the increase in the STH emission due to the neutron irradiation. This difference spectrum shows the neutron irradiation produces the most pronounced enhancement in the blue spectral region peaking at ~ 3.14 eV. The two blue bands have been reported in the literature and ascribed to donor-acceptor pair (DAP) recombination channels involving deep acceptors such as isolated $V_{Ga}$ and ($V_O$-$V_{Ga}$) defect pairs.[12,13] To improve the precision of the peak fitting method, the temperature dependence of the peak broadening of the defect-related BL peaks was included in the curve fitting process.[12]

CL data were also acquired from different depths within the crystal by increasing the acceleration voltage. The beam current was adjusted so that the beam power (17.3 μW) was kept constant to produce same e-h pair generation rate at each measurement voltage. The as-measured and normalized depth-resolved CL spectra for the pristine and irradiated crystals are shown in Fig. S4(a, b). The CL emission intensity is found to strengthen with increasing probe depth in both the pristine and irradiated crystals, suggesting that competitive non-radiative defects are present at the near surface region of the crystal most likely arising from residual surface polishing damage in the as-received sample. Notably, the normalized spectra reveal an identical peak shape and energy position with varying probe depth, which confirm both the UV and BL radiative centres are uniformly distributed throughout the crystal and doping homogeneity resulting from the neutron process.

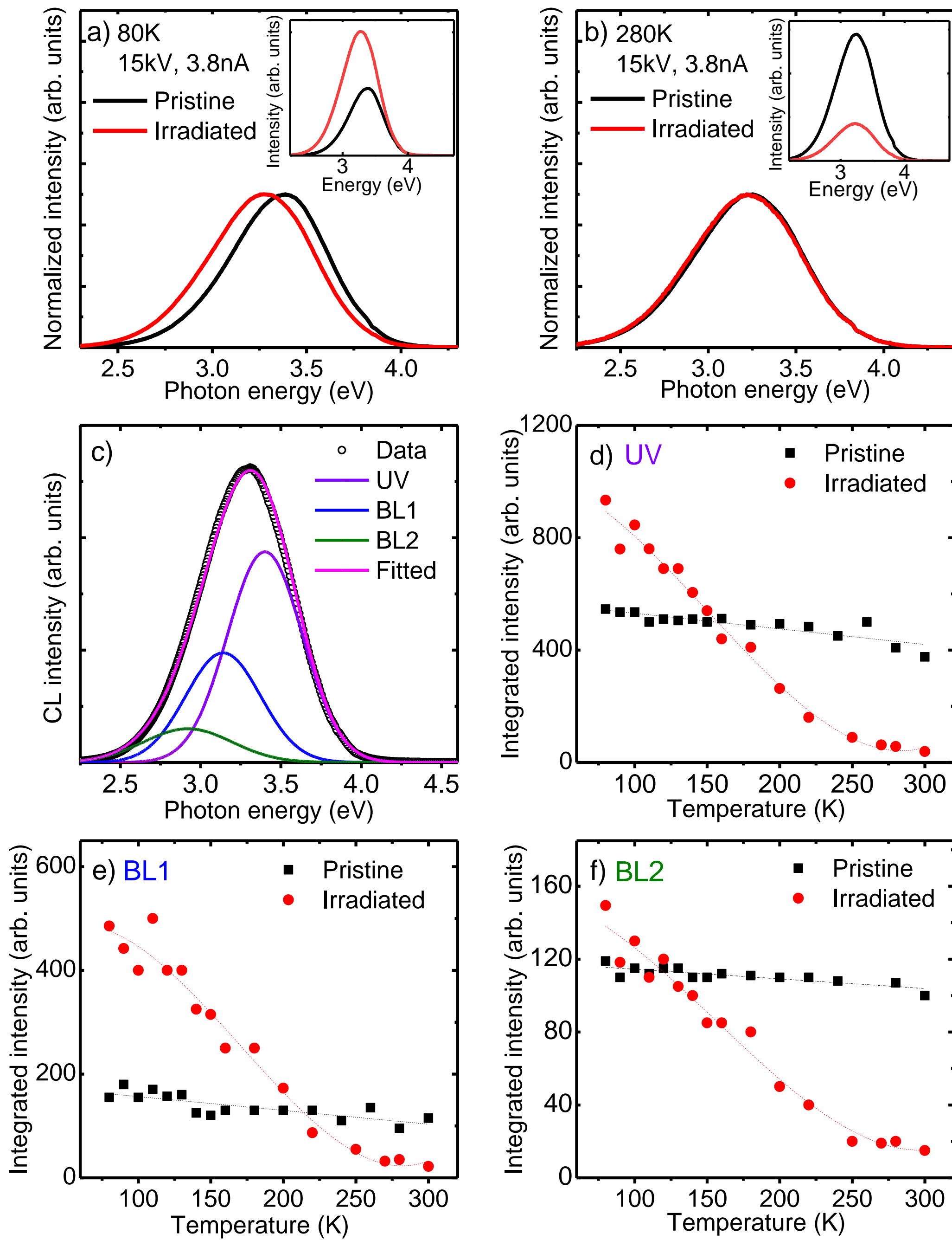


**Figure 2.** (a, b) Normalized CL spectra of the pristine and neutron-irradiated β-$Ga_2O_3$ acquired under identical excitation conditions at (a) 80 K and (b) 280 K. The creation of $V_{Ga}$ due to the neutron irradiation causes a red shift of 120 meV at 80 K, while the spectral shapes are identical at 280 K. The insets display the corresponding spectra before normalization, showing that the peak is enhanced at 80 K while it is quenched at 280 K. c) A typical fitted spectrum of the irradiated $Ga_2O_3$ at 80 K using three Gaussian peaks labelled UV (E = 3.40 eV, FWHM = 0.57 ± 0.03 eV), BL1 (3.14 eV, 0.55 ± 0.02 eV), and BL2 band (2.92 eV, 0.65 ± 0.02 eV). (d-f) Intensity versus temperature for the UV, BL1 and BL2 peaks in the pristine and irradiated β-$Ga_2O_3$ over the temperature range from 80 to 300 K. At 80 K, the intensity of the UV, BL1 and BL2 bands increases by a factor of 1.7, 3.2 and 1.3, respectively. With increasing temperature, the intensities of the all three bands in the irradiated β-$Ga_2O_3$ are quenched rapidly because the thermal activation of neutron-induced defects mediates the UV, BL1 and BL2 emission intensities.

Figure 2(d-f) shows plots of the CL intensity versus temperature between 80 and 300 K for the UV, BL1 and BL2 bands for the pristine and neutron-irradiated β-$Ga_2O_3$. The intensities of all three luminescence bands decrease with increasing temperature as competitive non-radiative transitions are thermally activated. However, a considerably faster decay is observed in the irradiated β-$Ga_2O_3$, suggesting that a highly efficient competitive non-radiative defect is created by the neutron irradiation that mediates the radiative recombination kinetics of the UV and BL bands in neutron irradiated $Ga_2O_3$. The enhancement of the blue bands in the irradiated β-$Ga_2O_3$ can be explained by the creation of $V_{Ga}$-related defects as a result of exposure to fast neutrons,[23,26] which leads to additional BL1 and BL2 recombination centers in the irradiated crystal. The luminescence behavior of the BL1 and BL2 bands upon the neutron irradiation and their temperature profiles are different [see Fig 2(e, f)], confirming they originate from different electronic transitions. Remarkably, the UV STH band is also enhanced at temperatures below 150 K upon the neutron irradiation, which suggests that the presence of $V_{Ga}$ can strongly influence the formation and stability of STHs in β-$Ga_2O_3$. Previous EPR studies revealed that ionized $V_{Ga}$ exhibits a hyperfine structure consistent with the localization of one or two holes on adjacent O atoms.[26] Consequently, the neutron-induced creation of $V_{Ga}$ defects can conceivably provide a mechanism to increase the hole concentration and so account for the increased UV STH emission post neutron irradiation. Also, the increase of $V_{Ga}$-related acceptors will compensate the irradiation induced n-type Ge doping, which explains the high electrical resistivity of the crystal after the neutron exposure.

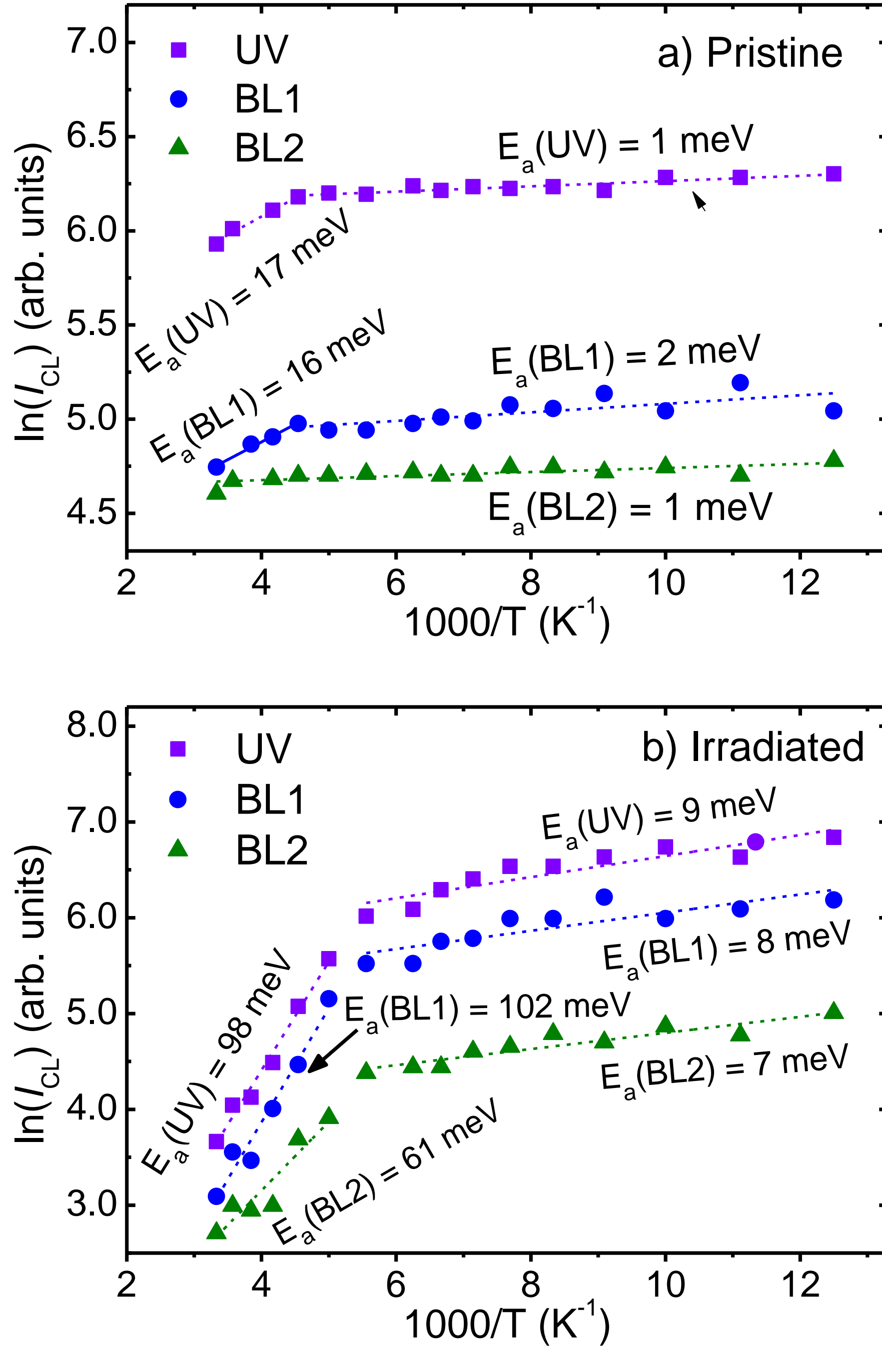


**Figure 3.** Arrhenius plots of ln ($I_{CL}$) versus 1000/K and linear analysis of the UV, BL1 and BL2 integrated intensities for (a) the pristine and (b) neutron-irradiated β-$Ga_2O_3$. Straight lines are fitted separately to lower and upper temperature ranges above and below 200 K, yielding the activation energies $E_a$ as indicated. The activation energies of the UV and BL1 bands are equivalent at 98 ± 6 meV for the irradiated β-$Ga_2O_3$, respectively, indicating the emission intensity bands are mediated by a new neutron-induced defect. In the low temperature range (< 200 K), all the emission bands possess much smaller activity energies, ~ 1 meV for the pristine crystal and ~ 8 meV for the irradiated crystal, which is most likely due to a phonon-assisted quenching process.

**Table 1**. Activation energies obtained from the Arrhenius analysis of the integrated peak intensity data for UV, BL1 and BL2 for temperatures above and below 200 K.

| | **Activation Energy (meV)** | |
|---|---|---|
| | *Pristine Crystal* | |
| **Peak** | Below 200 K | Above 200 K |
| UV 3.40 eV | 1.2 ± 0.2 | 17 ± 2 |
| BL1 3.14 eV | 2.0 ± 0.6 | 16 ± 1 |
| BL2 2.92 eV | 0.9 ± 0.2 | - |
| | *Neutron-Irradiated Crystal* | |
| UV 3.40 eV | 9.5 ± 1.5 | 98 ± 6 |
| BL1 3.14 eV | 8.2 ± 1.8 | 102 ± 10 |
| BL2 2.92 eV | 7.2 ± 1.6 | 62 ± 11 |

Arrhenius analysis of the UV, BL1 and BL2 bands is performed to determine the activation energy of their electronic transitions as illustrated in Fig. 3. The existence of two distinct linear temperature ranges extending from 80 to 200 K and 200 K to 300 K for both the pristine and neutron-irradiated $\beta$-$Ga_2O_3$ reveals the presence of two separate activation processes. Straight lines are fitted to each of the linear regions over lower and upper temperature ranges, yielding activation energies summarized Table 1. Below 200 K, the UV, BL1 and BL2 bands possess small activation energies at $E_a \approx 1$ and 8 meV for the pristine and irradiated $Ga_2O_3$, respectively. These weak temperature dependences of three luminescence bands are likely due to thermal quenching associated with a phonon-assisted excitation of localized defect states, similar to the mechanism observed in other oxides at low temperatures.[39] The activation energy of 17 meV above 200 K in the pristine crystal is within the binding energy range of 17 – 50 meV reported for shallow Sn and Si donors,[40] which are main impurities in EFG $\beta$-$Ga_2O_3$ crystals. Post neutron irradiation, the activation energy is

observed to increase to ~ 100 meV for the UV and BL1 bands and ~ 60 meV for the BL2 emission at temperatures beyond 200 K. The neutron irradiation induced increase of the CL emission is attributed to changes in the local deformation environment where holes are stabilized in the vicinity of an ionized $V_{Ga}$ defect.[26] Notably, the 100 meV activation energy in the neutron irradiated β-$Ga_2O_3$ is comparable with the previously reported ionisation energies of 110 meV for an unintentional donor in the EFG β-$Ga_2O_3$ crystal [8] and at 120 meV in Si-doped β-$Ga_2O_3$.[7] The chemical nature of this deep donor has not conclusively identified in the literature; possible origins include interstitials, antisites as well as Si or Ge occupying the octahedral Ga(II) site have been suggested to be responsible for this donor state.[8,10] The measured 100 meV activation energy is significantly smaller than the thermal activation energy of $Zn_{Ga}$ acceptors at both Ga(I) and Ga(II) sites, which is at least 0.65 eV.[41] This activation energy is also much smaller than the reported ionization energies of both $V_O$ and $V_{Ga}$,[42] thus these vacancy defects can be ruled out as its origin. Computational studies predict that the Si occupation is thermodynamically favorable on the Ga(I) over the Ga(II) site.[6] In contrast to equilibrium crystal growth techniques, Ge doping by neutron-induced Ga transmutation occurs under non-equilibrium conditions and Ge donors are incorporated on both Ga(I) and Ga(II) sites equally. Therefore, Ge(II) donors are abundant in neutron-induced Ge-doped β-$Ga_2O_3$ and their concentration in the irradiated crystal should be ~ $2.6 \times 10^{18}$ atoms/$cm^3$ from the ICP-MS results. By analogy to Si doping, Ge(II) donors would have similar ionization energy to the Si on a Ga(II) site, so accordingly the 100 meV activation energy measured after the neutron irradiation could be related to Ge donors on the Ga(II) site. It is plausible that the incorporated Ge in the irradiated crystal behaves like a localized DX-like donor state formed by the recoil of β particles in the decay of the Ga isotopes (see the decay equations in section III, part A). DX-like donor states have previously been identified in GaN after neutron irradiation,[18,43]

however, there are conflicting ESR [20] and electrical transport measurement [40] results that support and refute, respectively, the presence of DX-like donor states in β-$Ga_2O_3$.

The luminescence intensities of the CL bands in the β-$Ga_2O_3$ crystals were measured as a function of excitation density (beam current, $I_B$) before and after neutron irradiation. The UV and BL emissions were observed to exhibit remarkably similar excitation-power dependencies as $I_B$ was increased over three orders of magnitude from 0.1 nA to 10 nA while the beam energy was kept constant at $E_B = 15$ keV. Increasing $I_B$ in this range did not introduce any noticeable changes in peak shape or energy position [see Fig. S5(a, b)]. The power density analysis for the pristine and irradiated β-$Ga_2O_3$ crystals is illustrated in a log-log plot [Fig. S4(c, d)] using a simple power-law model $I_{CL} \propto I_B^k$, where $I_{CL}$ is the integrated peak intensity, $k$ is the power-law exponent and $I_B$ is the e-beam current. Power-law fits reveal identical $k$ values within the measurement error for the three bands with $k_{\text{pristine}} = 0.90 \pm 0.03$ and $k_{\text{irradiated}} = 0.99 \pm 0.02$ for the pristine and irradiated crystals, respectively. Power-law exponents around $k \cong 1$ are characteristic of excitonic and band-to-band transitions, which exhibit fast recombination rates. Conversely, recombination involving deep levels, such as free -to bound transitions, typically display much smaller $k$ values of ~ 0.5 due to their slow relaxation kinetics, arising from strong lattice coupling.[44] Accordingly, the measured $k \cong 1$ value for the BL1 and BL2 peaks is consistent with their assignment to DAP rather than free-to-bound transitions and provides an insight into the nature of the BL emission bands in $Ga_2O_3$.

A DAP emission band is comprised of multiple highly overlapped peaks each corresponding to each of the discrete lattice distances, $r$, between the donor and the acceptor involved in the radiative transition. The DAP emission energy is given by,[45,46]

$$h\nu(\text{DAP}) = E_g - (E_A + E_D) + \frac{e^2}{4\pi\epsilon\bar{r}} \qquad [1]$$

where $E_A$ and $E_D$ are the donor and acceptor binding energies, respectively. The last term accounts for the Coulombic interaction between the ionized donor and ionized acceptor with $r$ being their separation distance. Assuming a random distribution of donor-acceptor pairs, the average distance $\bar{r}$ can be estimated as $\bar{r} = \sqrt[3]{\frac{3}{4\pi N_{D/A}}}$, where $N_{D/A}$ is the higher $N_D$ or $N_A$ density.[46,47] Furthermore, the transition probability $P$(r) of the DAP pairs decreases exponentially with increasing $r$ as,

$$P(r) = P(r_{min})\, exp\left(-\frac{2\bar{r}}{r_B}\right), \quad [2]$$

where $r_B$ is the larger of the donor or acceptor Bohr radius.[48] Consequently, a DAP band typically blue shifts and changes shape with increasing $I_B$ since more distant pairs saturate more quicky than closer pairs and so no longer contribute the total DAP emission peak. The lack of a DAP blue shift with increasing excitation ($I_B$) can occur when predominantly close pairs are involved in the DAP transition. This can occur when either (i) the DAP involves a deep donor and a deep acceptor with highly localized wavefunctions or (ii) the donor and/or acceptor doping level is high reducing $\bar{r}$ and decreasing the DAP recombination lifetime, as described in Eq. 2. In this case, the latter reason applies since high concentrations of Ge, Sn and Si donors above $10^{17}$ $cm^{-3}$ exist in the crystal, as shown by ICP-MS. This DAP assignment is also consistent with the increase in the power-law exponent towards $k \approx 1$ post irradiation (see Fig. S5) as more $V_{Ga}$ acceptors are produced by fast neutrons.

An estimation of the donor concentration, $N_D$, in the Ge-doped $Ga_2O_3$ can be made using the energy position of the most enhanced BL1 peak at 3.14 eV due to the creation of neutron-induced $V_{Ga}$. Furthermore, for the production of $V_{Ga}$ and $Ga_i$ defect pairs via a knock-on effect by fast neutrons, all three $V_{Ga}^{i}$ split structural configurations are possible, with their acceptor energy $E_A$ in the range 1.62 – 1.69 eV.[15] Although the specific donor defect

responsible for the BL1 DAP transition in the irradiated $\beta$-$Ga_2O_3$ cannot be unequivocally identified, the logical candidate is transmuted Ge that acts as a shallow donor in the irradiated crystal. Using $E_D \approx 30$ meV for the donor energy of Si and Ge,[40,49] and $E_A \leq 1.69$ eV for the $V_{Ga}$ split configurations, equation [1] yields $\bar{r} \geq \sim 14$ nm, which corresponds to $N_D \leq 8 \times 10^{16}$ cm$^{-3}$. While the donor concentration of the neutron-irradiated crystal could not be measured using electrical measurements due to its high resistivity, this $N_D$ value is two orders of magnitude lower than the ICP-MS measured total Ge concentration of $5.2 \times 10^{18}$ atoms/cm$^3$, suggesting transmuted Ge donors are heavily compensated by irradiation-induced acceptors $V_{Ga}$ and $Zn_{Ga}$. Notably, previous studies showed Si-doped $Ga_2O_3$ epitaxial films with similar Si concentrations (up to $4 \times 10^{18}$ cm$^{-3}$) were still non-conducting electrically.[50] The second blue band $BL_2$ at ~2.9 eV has been previously attributed to DAP involving $V_{Ga}$-related acceptors in single crystals [51] or $Zn_{Ga}$ acceptors in Zn-doped $Ga_2O_3$.[36] However, our experimental results do not support the involvement of $V_{Ga}$ as the $BL_2$ intensity only exhibits a modest intensity increase post neutron irradiation at temperatures below 120 K even though the irradiation produces a substantial increase in the $V_{Ga}$ concentration. The electrical conductivity of $\beta$-$Ga_2O_3$ was previously found to decrease while the photocurrent in $\beta$-$Ga_2O_3$ Schottky diodes increased after exposure to fast neutrons; these findings were ascribed to the creation of predominantly $V_{Ga}$ defects by fast neutrons.[27,52] It is likely that the $BL_2$ DAP involves either $V_O$ donors or ($V_O$-$V_{Ga}$) acceptor complexes because the concentration of these defects will remain unchanged after the neutron irradiation. The higher $BL_2$ recombination rate with its $k$ value raising from 0.87 to 0.99 post irradiation (see Fig. S5), together with the ICP-MS Ge doping results, suggests that the $BL_2$ DAP could arise from Si / Ge donors and ($V_O$-$V_{Ga}$) acceptor complexes, as defined by Eq. 2. However, further work is required to confirm these defect assignments. Thermal annealing at temperatures up to 700°C in argon was attempted to remove the neutron irradiation-induced vacancies in the crystal but was found to

be ineffective as no changes in the luminescent and electrical properties were detected after the annealing treatment. This result suggests that $V_{Ga}$ and other defects produced by neutron irradiation exhibit a high thermal stability.

## IV. CONCLUSIONS

Neutron irradiation and chemical analyses in this work show that thermal neutron irradiation can be used to incorporate Ge donors into β-$Ga_2O_3$ by the transmutation decay of lattice Ga cations that have captured thermal neutrons. This finding potentially opens the door for uniform Ge doping, where the concentration can be precisely controlled by varying the irradiation period and post-irradiation time. However, neutron irradiation also creates $V_{Ga}$ and $Zn_{Ga}$ acceptors, reducing the carrier density. Furthermore, the intensity of the STH UV emission at 80 K is enhanced by approximately twofold post neutron irradiation; this enhancement indicates that neutron-induced $V_{Ga}$ centers can stabilize holes in β-$Ga_2O_3$ and supports the theoretically predicted model of holes being trapped at O ions adjacent to a Ga vacancy. The most pronounced CL enhancement due to the neutron irradiation is the blue DAP band at 3.14 eV, where the donor is a shallow Ge donor state, and the acceptor is a $Ga_i$-$V_{Ga}$ pair complex. Significantly, this blue band and STH UV emission in the irradiated β-$Ga_2O_3$ exhibit identical temperature dependencies with a similar activation energy of ~100 meV, indicating that the intensities are mediated by an efficient non-radiative defect, which is likely a DX-like Ge center in which Ge is situated at the octahedral Ga(II) site. This non-radiative defect acts as a competitive recombination center that controls the recombination kinetics in neutron Ge-doped $Ga_2O_3$. Our findings illustrate the importance of using an array of complementary characterization techniques to fully understand the neutron transmutation doping process in $Ga_2O_3$.

## Acknowledgements

This work was supported under Australian Research Council (ARC) Discovery Project funding scheme (project DP210101146). The authors acknowledge the support of ANSTO in providing access to the neutron irradiation facility used in this work via Proposal AP12165 and thank Herbert Yuan for technical support with SEM analysis.

## References

[1] S. J. Pearton, J. Yang, P. H. Cary IV, F. Ren, J. Kim, M. J. Tadjer, and M. A. Mastro, Appl. Phys. Rev. **5**, 011301 (2018).

[2] T. T. Huynh, E. Chikoidze, C. P. Irvine, M. Zakria, Y. Dumont, F. H. Teherani, E. V. Sandana, P. Bove, D. J. Rogers, M. R. Phillips, and C. Ton-That, Phys. Rev. Mater. **4**, 085201 (2020).

[3] M. Higashiwaki, K. Sasaki, T. Kamimura, M. H. Wong, D. Krishnamurthy, A. Kuramata, T. Masui, and S. Yamakoshi, Appl. Phys. Lett. **103**, 123511 (2013).

[4] K. Irmscher, Z. Galazka, M. Pietsch, R. Uecker, and R. Fornari, J. Appl. Phys. **110**, 063720 (2011).

[5] N. Moser, J. McCandless, A. Crespo, K. Leedy, A. Green, A. Neal, S. Mou, E. Ahmadi, J. Speck, K. Chabak, N. Peixoto, and G. Jessen, Ieee Electron Device Letters **38**, 775 (2017).

[6] J. B. Varley, J. R. Weber, A. Janotti, and C. G. Van de Walle, Appl. Phys. Lett. **97**, 142106 (2010).

[7] Z. Feng, A. Anhar Uddin Bhuiyan, M. R. Karim, and H. Zhao, Appl. Phys. Lett. **114**, 250601 (2019).

[8] A. T. Neal, S. Mou, R. Lopez, J. V. Li, D. B. Thomson, K. D. Chabak, and G. H. Jessen, Scientific Reports **7**, 13218 (2017).

[9] S.-S. Huang, R. Lopez, S. Paul, A. T. Neal, S. Mou, M.-P. Houng, and J. V. Li, Japanese Journal of Applied Physics **57**, 091101 (2018).

[10] K. Iwaya, R. Shimizu, H. Aida, T. Hashizume, and T. Hitosugi, Appl. Phys. Lett. **98**, 142116 (2011).

[11] Y. S. Wang, P. T. Dickens, J. B. Varley, X. J. Ni, E. Lotubai, S. Sprawls, F. Liu, V. Lordi, S. Krishnamoorthy, S. Blair, K. G. Lynn, M. Scarpulla, and B. Sensale-Rodriguez, Sci. Rep. **8**, 18075 (2018).

[12] T. T. Huynh, L. L. C. Lem, A. Kuramata, M. R. Phillips, and C. Ton-That, Phys. Rev. Mater. **2**, 105203 (2018).

[13] T. Onuma, S. Fujioka, T. Yamaguchi, M. Higashiwaki, K. Sasaki, T. Masui, and T. Honda, Appl. Phys. Lett. **103**, 041910 (2013).

[14] L. Binet and D. Gourier, J. Phys. Chem. Solids **59**, 1241 (1998).

[15] M. E. Ingebrigtsen, A. Y. Kuznetsov, B. G. Svensson, G. Alfieri, A. Mihaila, U. Badstubner, A. Perron, L. Vines, and J. B. Varley, Apl Materials **7**, 022510 (2019).

[16] A. Karjalainen, V. Prozheeva, K. Simula, I. Makkonen, V. Callewaert, J. B. Varley, and F. Tuomisto, Physical Review B **102**, 195207 (2020).

[17] J. M. Johnson, Z. Chen, J. B. Varley, C. M. Jackson, E. Farzana, Z. Zhang, A. R. Arehart, H. L. Huang, A. Genc, S. A. Ringel, C. G. Van de Walle, D. A. Muller, and J. Hwang, Physical Review X **9**, 041027 (2019).

[18] K. Kuriyama, T. Tokumasu, J. Takahashi, H. Kondo, and M. Okada, Appl. Phys. Lett. **80**, 3328 (2002).

[19] A. Polyakov, N. Smirnov, A. Govorkov, A. Markov, S. Pearton, N. Kolin, D. Merkurisov, V. Boiko, C.-R. Lee, and I.-H. Lee, Journal of Vacuum Science & Technology B: Microelectronics and Nanometer Structures Processing, Measurement, and Phenomena **25**, 436 (2007).

[20] N. Son, K. Goto, K. Nomura, Q. Thieu, R. Togashi, H. Murakami, Y. Kumagai, A. Kuramata, M. Higashiwaki, and A. Koukitu, J. Appl. Phys. **120**, 235703 (2016).

[21] S. Bhandari, C. Nardone, and M. Zvanut, J. Appl. Phys. **132**, 025701 (2022).

[22] M. E. Ingebrigtsen, J. B. Varley, A. Y. Kuznetsov, B. G. Svensson, G. Alfieri, A. Mihaila, U. Badstubner, and L. Vines, Appl. Phys. Lett. **112**, 042104 (2018).

[23] E. Farzana, M. F. Chaiken, T. E. Blue, A. R. Arehart, and S. A. Ringel, Apl Materials **7**, 022502 (2019).

[24] M. Chang, D. Guo, X. Zhong, F. Zhang, and J. Wang, J. Appl. Phys. **132**, 123105 (2022).

[25] H. Gao, S. Muralidharan, N. Pronin, M. R. Karim, S. M. White, T. Asel, G. Foster, S. Krishnamoorthy, S. Rajan, L. R. Cao, M. Higashiwaki, H. Wenckstern, M. Grundmann, H. Zhao, D. C. Look, and L. J. Brillson, Appl. Phys. Lett. **112**, 242102 (2018).

[26] B. E. Kananen, L. E. Halliburton, K. T. Stevens, G. K. Foundos, and N. C. Giles, Appl. Phys. Lett. **110**, 202104 (2017).

[27] E. Yakimov, A. Polyakov, I. Shchemerov, N. Smirnov, A. Vasilev, P. Vergeles, E. Yakimov, A. Chernykh, A. Shikoh, and F. Ren, APL Materials **8**, 111105 (2020).

[28] H. T. Gao, S. Muralidharan, M. R. Karim, S. M. White, L. R. Cao, K. Leedy, H. P. Zhao, D. C. Look, and L. J. Brillson, J. Phys. D Appl. Phys. **53**, 465102 (2020).

[29] A. Kuramata, K. Koshi, S. Watanabe, Y. Yamaoka, T. Masui, and S. Yamakoshi, Jpn. J. Appl. Phys. **55**, 1202a2 (2016).

[30] S. J. Kennedy, Phys. B: Condens. Matter. **385**, 949 (2006).

[31] H. Meriaty, Characterisation of the neutron field at the ANSTO instrument calibration facility, Australian Nuclear Science & Technology Organisation, ANSTO, Australia, 2009.

[32] C. H. Seager and T. G. Castner, J. Appl. Phys. **49**, 3879 (1978).

[33] M. A. Vesaghi, Phys. Rev. B **25**, 5436 (1982).

[34] https://www.nndc.bnl.gov.

[35] See Supplemental Material at xxx for additional characterization results.

[36] I. López, M. Alonso-Orts, E. Nogales, and B. Méndez, Phys. Status Solidi A **215**, 1800217 (2018).

[37] S. Yamaoka, Y. Mikuni, and M. Nakayama, J. Phys. Conf. Ser. **1220**, 012030 (2019).

[38] K. Shimamura, E. G. Víllora, T. Ujiie, and K. Aoki, Appl. Phys. Lett. **92**, 201914 (2008).

[39] Z. Lin, W. Chen, R. Zhan, Y. Chen, Z. Zhang, X. Song, J. She, S. Deng, N. Xu, and J. Chen, AIP Advances **5**, 107229 (2015).

[40] A. T. Neal, S. Mou, S. Rafique, H. P. Zhao, E. Ahmadi, J. S. Speck, K. T. Stevens, J. D. Blevins, D. B. Thomson, N. Moser, K. D. Chabak, and G. H. Jessen, Appl. Phys. Lett. **113**, 062101 (2018).

[41] T. D. Gustafson, J. Jesenovec, C. A. Lenyk, N. C. Giles, J. S. McCloy, M. McCluskey, and L. E. Halliburton, J. Appl. Phys. **129**, 155701 (2021).

[42] T. Lovejoy, R. Chen, X. Zheng, E. Villora, K. Shimamura, H. Yoshikawa, Y. Yamashita, S. Ueda, K. Kobayashi, and S. Dunham, Appl. Phys. Lett. **100**, 181602 (2012).

[43] P. Boguslawski and J. Bernholc, Physical Review B **56**, 9496 (1997).

[44] C. Ton-That, L. Weston, and M. R. Phillips, Phys. Rev. B **86**, 115205 (2012).

[45] D. G. Thomas, J. J. Hopfield, and W. M. Augustyniak, Phys. Rev. **140**, A202 (1965).

[46] K. Thonke, T. Gruber, N. Teofilov, R. Schonfelder, A. Waag, and R. Sauer, Physica B **308**, 945 (2001).

[47] F. Williams, Phys. Status Solidi B **25**, 493 (1968).

[48] A. Vink, Journal of Luminescence **9**, 159 (1974).

[49] T. Jiao, Z. Li, W. Chen, X. Dong, Z. Li, Z. Diao, Y. Zhang, and B. Zhang, Coatings **11**, 589 (2021).

[50] D. Gogova, G. Wagner, M. Baldini, M. Schmidbauer, K. Irmscher, R. Schewski, Z. Galazka, M. Albrecht, and R. Fornari, J. Cryst. Growth **401**, 665 (2014).

[51] T. Onuma, Y. Nakata, K. Sasaki, T. Masui, T. Yamaguchi, T. Honda, A. Kuramata, S. Yamakoshi, and M. Higashiwaki, J. Appl. Phys. **124**, 075103 (2018).

[52] L. Cojocaru, Radiat. Eff. **21**, 157 (1974).